PHYSICAL REVIEW B **90**, 241408(R) (2014)

Stability and properties of high-buckled two-dimensional tin and lead

Pablo Rivero,[1] Jia-An Yan,[2] Víctor M. García-Suárez,[3] Jaime Ferrer,[3] and Salvador Barraza-Lopez[1,*]

[1]*Department of Physics, University of Arkansas, Fayetteville, Arkansas 72701, USA*

[2]*Department of Physics, Astronomy and Geosciences, Towson University, Towson, Maryland 21252, USA*

[3]*Departamento de Física and Centro de Investigación en Nanociencia y Nanotecnología, Universidad de Oviedo, 33003 Oviedo, Asturias, Spain*

(Received 27 July 2014; revised manuscript received 17 November 2014; published 5 December 2014)

In realizing practical nontrivial topological electronic phases stable structures need to be determined first. Tin and lead do stabilize an optimal two-dimensional high-buckled phase—a hexagonal close-packed bilayer structure with ninefold atomic coordination—and they do not stabilize topological fullerenes, as demonstrated by energetics, phonon dispersion curves, and structural optimization of finite-size samples. The high-buckled phases are metallic due to their high atomic coordination. The optimal structure of fluorinated tin lacks threefold symmetry and it stabilizes small samples too. It develops two oblate conical valleys in the first Brillouin zone coupling valley, sublattice, and spin degrees of freedom with a novel $\tau_z\sigma_x s_x$ term, thus making it a new two-dimensional platform for valleytronics.

DOI: 10.1103/PhysRevB.90.241408 PACS number(s): 73.22.−f, 68.55.at, 71.70.Ej

Introduction. Carbon forms two-dimensional (2D) layers with a hexagonal lattice [1,2], and silicon, germanium [3], AlAs, AlSb, GaP, InP, GaAs, InAs, GaSb, InSb [4], phosphorus [5], and tin [6–8] are all predicted to form stable low-buckled (LB) 2D hexagonal layers. High-buckled (HB) 2D phases cannot occur for carbon, silicon, or germanium [3,9]. Can tin and lead stabilize the HB phase?

Proceeding by direct analogy to silicene and germanene [3], known studies of the electronic properties of 2D tin [6–8,10] are performed under the implicit assumption that the HB phase is not viable. In addition, the guess structures and the electronic gaps in Ref. [8] had been previously reported [7]. Contrary to common assumption, the HB 2D structures of the heavy column IV elements tin and lead are stable and lower in energy than their LB counterparts, thus representing the true optimal structures of these 2D systems. The structural stability of HB tin and HB lead will have fundamental consequences for the practical realization of substrate-free nontrivial topological phases based on these elements.

The optimal phase of 2D fluorinated stanene is not analogous to tetrahedrally coordinated graphane [11] as postulated in Refs. [7] and [8]. Studies of 2D fluorinated tin dismiss the existence of bulk crystalline fluorinated phases stable at room temperature. *There is no indication of tetrahedral coordination of tin atoms* in bulk fluorinated tin [12], and tetrahedral coordination [7,8] does not yield the most stable 2D fluorinated tin either.

We uncover *six metastable fluorinated phases for 2D tin*, the graphane-like phase [6–8] being one of them. Consistent with the literature on bulk flourinated tin [12,13], we demonstrate that *two tilted F atoms mediate the interaction among two Sn atoms* in the optimal 2D structure. This stable optimal phase displays two gapped oblate Dirac cones in the first Brillouin zone, where valley $\boldsymbol{\tau}$, pseudospin $\boldsymbol{\sigma}$, and spin $\mathbf{s}$ couple as $\tau_z\sigma_x s_x$ [14].

Unlike known 2D materials with a hexagonal lattice, in which three valleys with momentum directions separated by 120° rotations are related due to threefold symmetry [15–19], the optimal 2D fuorinated tin leads to *strictly two* valleys due to its reduced structural symmetry. This allows an unprecedented specificity in coupling three quantum degrees of freedom around the Fermi energy: the valley, the crystal momentum *including direction*, and the electronic spin. The results provided here invite to look closely into 2D materials postulated for their remarkable electronic properties that may not realize ground-state, optimal structures [7,8].

The HB phase is more favorable than the LB phase with increasing atomic number: The energetics of column IV 2D materials in Fig. 1(a) were obtained with the PBE exchange-correlation potential [20] in a version of the SIESTA code [21,22] that includes a self-consistent spin-orbit interaction (SOI) [23]. Our basis sets are of double-ζ plus polarization size [24]. The trends in Fig. 1 remain regardless of the inclusion of SOI and were cross-checked with VASP calculations [25,26].

The lattice constant at the HB energy minima a_{HB} is equal to 3.418 Å for tin, and $a_{\mathrm{HB}} = 3.604$ Å for lead. These values become 3.413 and 3.575 Å, respectively, when the SOI is included in calculations. These strikingly stable HB structures have not been reported before; lattice parameters in the literature [6–8,10] are ∼140% larger. The normalization of a_0 in terms of a_{HB} in Figs. 1(a) facilitates a unified display of energetics regardless of the atomic species. The dashed vertical line in Figs. 1(a) and 1(b) at about $a_0 \simeq 1.2a_{\mathrm{HB}}$ highlights the lattice constant a_0 for which energy barriers separating the LB and the HB phases become largest.

Germanium (with atomic number $Z = 32$) cannot form an HB phase, even though the energy minimum of the optimized HB phase is already lower than the local minimum at the optimal LB phase [Fig. 1(a)] [3]. This HB minimum becomes markedly deeper and the energy barriers separating these phases become shallower with increasing atomic number. Figure 1(a) invites us to ponder whether HB tin and HB lead are stable. In answering this question we address the atomistic coordination of HB phases first.

The optimal HB structure is a hexagonal close-packed (HCP) bilayer: HB phases have been represented as threefold coordinated [3], but the relative height Δz among atoms

*sbarraza@uark.edu

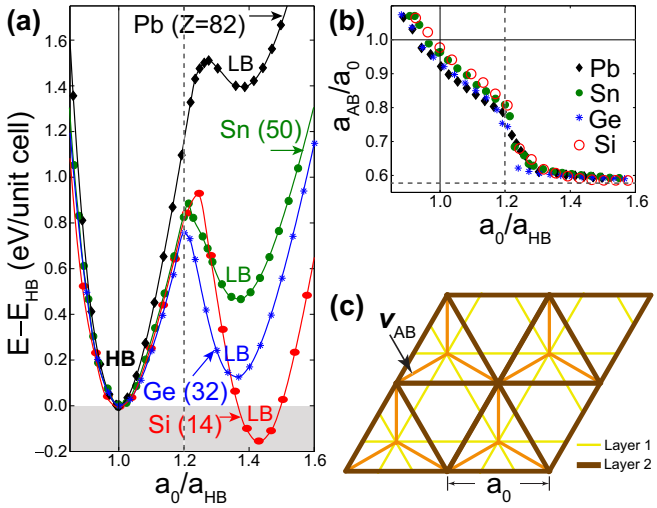

FIG. 1. (Color online) (a) The high-buckled phase becomes more stable with increasing atomic number. (b) Nearest-neighbor distances $a_{AB} \equiv |\mathbf{v}_{AB}|$ approach the lattice constant a_0 ($a_{AB} \simeq a_0$) at the high-buckled energy minimum; the structure transitions to a low-buckled phase at roughly $1.2a_{\mathrm{HB}}$. (c) The high-buckled structure is an HCP bilayer.

in complementary sublattices A and B increases as the lattice constant a_0 is compressed, so the distance $a_{AB} = \sqrt{a_0^2/3 + \Delta z^2}$ among atoms belonging to complementary sublattices increases towards a_0. Indeed, $a_{AB} = a_0/\sqrt{3}$ for a planar hexagonal unit cell [dashed horizontal line in Fig. 1(b)] but an ideal HCP structure has $\Delta z = \sqrt{2}a_0/\sqrt{3}$, yielding $a_{AB} = a_0$ [solid horizontal line in Fig. 1(b)] [27]. Numerical results yield $a_{AB} \simeq 0.95a_{\mathrm{HB}}$ [solid vertical line in Fig. 1(b)]. Thus, six atoms are a distance a_{HB} apart and three atoms belonging on complementary sublattices are separated by $a_{AB} \simeq 0.95a_{\mathrm{HB}}$, leading to the ninefold-coordinated HCP bilayer structure [28,29] in Fig. 1(c). A transition among LB and HB structures occurs around $a_0 \simeq 1.2a_{\mathrm{HB}}$ in Fig. 1(b).

HB tin and HB lead are stable: We show in Figs. 2(a) and 2(b) phonon dispersion curves for HB tin and lead [30]. The effect of SOI is small, thus justifying the trends without SOI shown in Figs. 1(a) and 1(b) [31]. Similar dispersions were obtained using the QUANTUM ESPRESSO code [32]. The lack of significant negative energies indicates that HB tin and HB lead are indeed stable: The chemistry of Si and Ge does not translate to Sn and Pb because, with increasing atomic number, the s orbital lowers its energy with respect to the p orbital, thus reducing $s - p$ hybridization.

The ultimate test of relative stability is a structural optimization of small 2D flakes with initial HB or LB conformations [Fig. 2(c)], where the lines joining atoms reveal their atomistic coordination. The finite-size HB structures have 122 atoms; the LB structures have eight additional atoms [small filled (red) circles in the LB initial structure] so that all edge atoms are twofold coordinated. We set a stringent force tolerance cutoff of at least 0.01 eV/Å.

The LB Si and LB Ge samples [Fig. 2(c), subplots ii and iv] show crumpling originating out from the boundaries yet the hexagonal lattice remains visible around the center of mass after the force relaxation [3]. On the other hand, the amorphous shape and the random-looking atomistic coordination of HB Si and HB Ge (subplots i and iii) indicate that these phases are unstable [3].

Confirming the structural stability inferred from phonon dispersion curves, HB Sn and HB Pb do stabilize in finite-size samples: Starting from an ideal HB phase, the optimized Sn structure retains the HB coordination within the area highlighted by the large black oval [Fig. 2(c), subplot v]. The finite LB Sn sample, on the other hand, crumples upon optimization [Fig. 2(c), subplot vi]. In fact, the region highlighted by the small black oval in Fig. 2(c), subplot vi, displays the local coordination expected of an HB phase already. Similar conclusions would be reached in Ref. [10] if periodic constraints were removed.

Haldane's honeycomb model has been studied in closed geometries [33] and one of the many candidates for its practical realization is LB tin (stanene). Unfortunately, a fullerene-like Sn_{60} is not stable [Fig. 2(d)] so tin and lead are no-go elements for topological fullerenes. Based on Fig. 1(a) HB lead is extremely stable: It stabilizes finite HB samples with no change

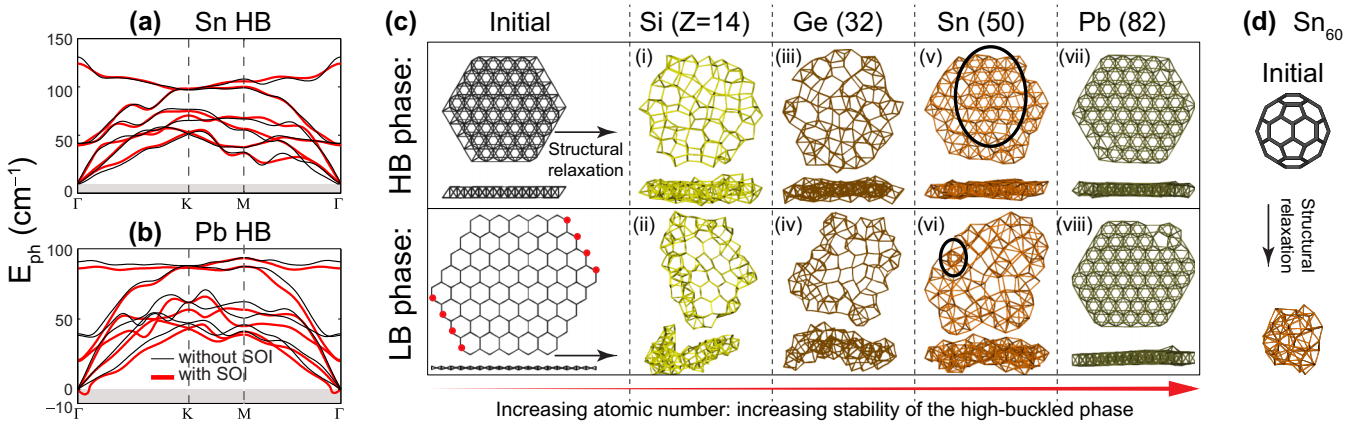

FIG. 2. (Color online) (a, b) Phonon dispersions $E_{\mathrm{ph}}(\mathbf{k})$ for HB tin and lead demonstrate their structural stability; SOI does not change phonon dispersions dramatically. (c) The structural optimization of finite samples reflects previous findings for Si and Ge [3] and helps to confirm the stability of HB tin and HB lead unequivocally: The stanene sample (LB tin) becomes thick and amorphous and the initial LB lead sample turns into HB lead. (d) Two-dimensional tin and lead do not realize topological fullerenes.

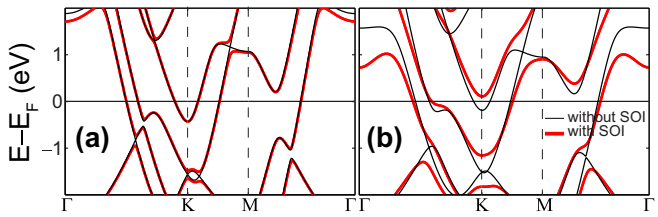

FIG. 3. (Color online) Electronic dispersion for (a) HB tin and (b) HB lead. The ninefold atomic coordination of the HB phases is behind the metallic electronic dispersion.

in atomic coordination [Fig. 2(c), subplot vii] and turns an LB structure into an HB-coordinated one [Fig. 2(c), subplot viii].

Viable electronic materials require stable structures. Tin and lead films have been created experimentally [38–40] and structural aspects must be addressed diligently to realize 2D materials with a strong SOI.

Graphene, silicene, and germanene are threefold coordinated and have a conical dispersion around the K points, with small gaps due to SOI [14,34–37]. The ninefold-coordinated 2D HB structures display no conduction gaps (Fig. 3).

HCP bilayers could be cleaved out of HCP or FCC bulk structures. Lead forms an FCC structure with interatomic distances of 3.614 Å, which compare favorably with $a_{\mathrm{HB}} = 3.575$ and make HB lead stable.

Tin stabilizes a tetragonal structure (β tin [41,42]) and a diamond structure (α tin [43]). The β phase is higher in energy than the α phase by $E_\beta - E_\alpha = 0.58$ eV/atom. Every atom in

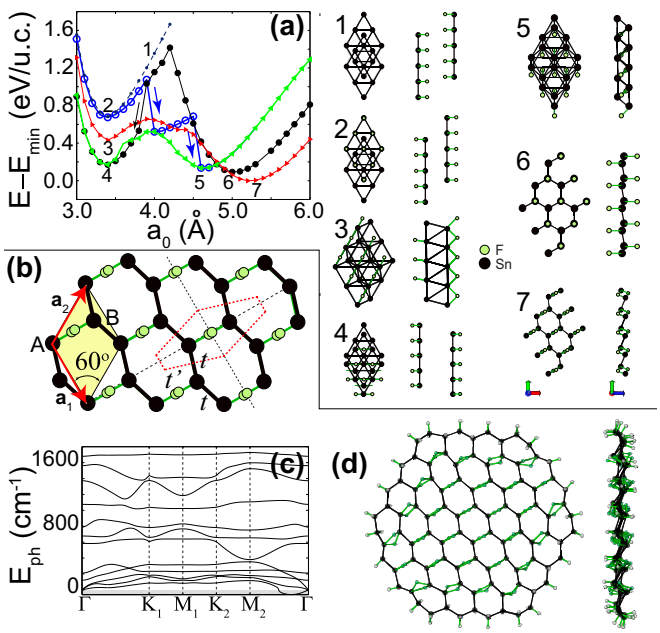

FIG. 4. (Color online) (a) Phases of 2D fluorinated tin; structures are shown at the right. (b) Symmetries of the most stable structure, (7), depicting triangular (dashed lines) and Wigner-Seitz (within the dotted perimeter) unit cells, the two symmetry axes, and the two Sn sublattices, A and B. Structural stability is demonstrated by (c) the phonon dispersion curves and (d) the structural stabilization of a finite-size sample.

β tin has 4 neighbors 3.11 Å apart, 2 neighbors 3.26 Å apart, and 4 neighbors 3.87 Å apart: these 10 atoms are 3.44 Å apart on average. In ninefold-coordinated HB tin $a_{\mathrm{HB}} = 3.42$ Å and $a_{AB} = 3.281$, having an atomistic coordination comparable to that of bulk β tin. The α-tin phase has four neighbors 2.89 Å apart, which compares well to the $a_{\mathrm{Sn\text{-}Sn}} = 2.85$ Å for a 2D LB structure. Importantly, in two dimensions the energetics switch and the HB phase—compatible with bulk β tin—is more stable than LB tin—compatible with α tin—by $E_{\mathrm{LB}} - E_{\mathrm{HB}} = 0.25$ eV/atom [cf. Fig. 1(a)].

The phase space for decorated 2D tin is larger than originally anticipated [Fig. 4(a)]: The graphane-like phase [7,8] realizes the metastable minimum labeled **6**, which turns into phase **4** upon in-plane compression. Placement of F atoms directly on top of/under Sn atoms results in two dissociated triangular Sn lattices bonded on opposite sides by F atoms (structures **2**/**1**).

In the optimal structure, **7**, fourfold-coordinated Sn atoms form a sequence of parallel zigzag 1D chains, with two fluorine atoms mediating interactions among neighboring Sn chains. The structure is realized on a triangular lattice with $a_0 = 5.230$ Å [Fig. 4(b)]. The Wigner-Seitz unit cell is within

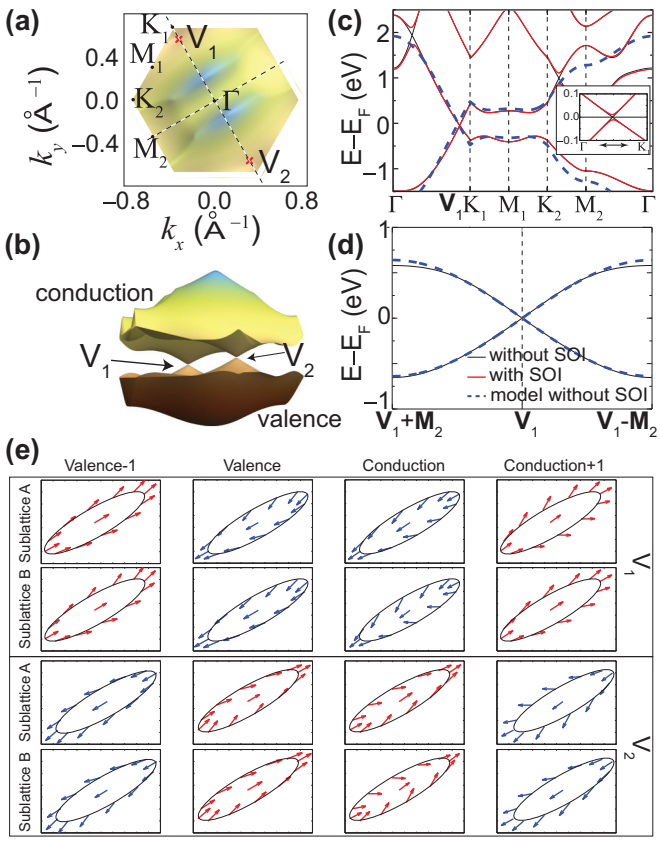

FIG. 5. (Color online) (a) Conduction band in the first Brillouin zone, highlighting high-symmetry points and locations of valleys $\mathbf{V}_1$ and $\mathbf{V}_2$ away from the K and K' points. (b) The two valleys in the Brillouin zone arise from the twofold symmetry of the atomic structure. (c, d) Band structures along high-symmetry lines, including a two-band tight-binding fit. (e) Spin texture resolved over valley ($\boldsymbol{\tau}$), energy, and sublattice ($\boldsymbol{\sigma}$) degrees of freedom. (The spin projection onto the z axis is of the order of 1% at most.)

TABLE I. Basis vectors for the optimal fluorinated 2D tin ($a_0 = 5.23$ Å).

Sn	$(0.000, 0.000, 0.000)a_0$,	$(0.583, 0.336, -0.221)a_0$
F	$(0.216, 0.124, -0.348)a_0$,	$(0.367, 0.212, 0.128)a_0$

the dotted area in Fig. 4(b); the symmetry axes are shown as well. A similar "bridging" fluorine coordination is realized in bulk tin(II) fluoride (e.g., Fig. 2 in Ref. [12]).

Bulk tin(II) fluoride is highly stable at room temperature and can be found in household products. The structural stability of optimal 2D tin is probed with phonon dispersion calculations [Fig. 4(c)] along the high-symmetry lines shown in Fig. 5(a). The phonon frequency range is comparable with that of graphene, and it is one order of magnitude larger than those in Figs. 2(a) and 2(b). As an additional successful check, small-size flakes were subjected to a successful structural optimization [Fig. 4(d)]. The peculiar coupling of quantum degrees of freedom in this system may encourage experimental routes towards the synthesis of 2D fluorinated tin. The stability of its parent 3D compound at room temperature [12,13] invites experimental investigations of potential viability in two dimensions.

The first Brillouin zone in Fig. 5(a) shows a top view of the conduction band and the high-symmetry points in momentum space. As shown in Fig. 5(b), the arrangement of parallel 1D Sn wires gives rise to an electronic structure with only two anisotropic Dirac cones in the first Brillouin zone, located away from the K points at positions $\mathbf{V}_1$ and $\mathbf{V}_2 = \pm 0.85\mathbf{K}_1$, respectively. Henceforth we identify the x axis with the line joining tin atoms across fluorine bridges. The Fermi velocity is close in magnitude to that of graphene and it is anisotropic—$v_{Fy} = 5.4 \times 10^5$ m/s [Fig. 5(c)], and $v_{Fx} = 2.1 \times 10^5$ m/s [Fig. 4(d)]—and a gap of $2\Delta = 0.02$ eV opens due to SOI, five times larger than the intrinsic gap due to SOI in graphene [35]. Phase **6** transitions from a topological insulator to a trivial insulator [8], but the electronic structure of the optimal phase remains robust under even larger isotropic strain.

The electronic dispersion in Figs. 5(b)–5(d) can be understood in terms of a 2×2 π-electron tight-binding Hamiltonian [44] in which an effective coupling t' is set among the tin atoms originally linked by fluorine bridges [thin bonds in Fig. 4(b)], and t is the coupling among actual Sn-Sn atoms [thick bonds in Fig. 4(b)]. Using interatomic distances among Sn atoms from Table I, $t = 0.8$ eV and $t' = v_{Fx}t/v_{Fy}$, we obtain the (blue) dashed lines in Figs. 5(c) and 5(d), which reproduce first-principles results.

To account for SOI, we realize an oblate low-energy Dirac-Hamiltonian at the vicinity of the $\mathbf{V}_{1,2}$ points. The relevant subspace is four-dimensional at any given valley, and the task is to reproduce the spin texture displayed in Fig. 5(e), where spin projects onto the $+x$ or the $-x$ direction while leaving the sublattice (pseudospin) degree of freedom unpolarized. The numerical results in Fig. 5(e) are consistent with the coupling $\tau_z\sigma_x s_x$. Indeed, eigenvectors of $\tau_z\sigma_x s_x$ in Table II project spins onto the $-x, +x, +x, -x$ axis parallel to the Sn-F bonds, inverting the signs at each valley and lacking sublattice polarization, consistent with *ab initio* data [Fig. 5(e)]. Thus, the low-energy dynamics is given by

$$H = -i\hbar\Psi^\dagger(v_{Fx}\tau_z\sigma_x\partial_x + v_{Fy}\sigma_y\partial_y)\Psi + \Psi^\dagger(\Delta\tau_z\sigma_x s_x)\Psi.$$

An unprecedented specific coupling of momentum—including direction—with spin oriented along $\hat{\mathbf{x}}$ and valley degrees of freedom is thus realized by the second term in previous equation. The valley degree of freedom can be addressed by a bias along the $\mathbf{V}_1 - \mathbf{V}_2$ axis that breaks inversion symmetry. Similarly, a magnetic field along the $\hat{\mathbf{x}}$ axis will break time-reversal symmetry, locking the valley and crystal momentum direction at the $\mathbf{V}_1$, $\mathbf{V}_2$ points. The dynamics invites the use of 2D fluorinated tin for valleytronic applications.

TABLE II. Eigenvectors of $\tau_z\sigma_x s_x$. $|s_x;\pm\rangle$ are eigenstates of s_x, and $|A\rangle$, $|B\rangle$ are eigenstates of the pseudospin (sublattice projection) operator.

State	V_1	V_2
$\|\phi_{-\Delta,1}\rangle$	$\frac{1}{\sqrt{2}}(-\|A\rangle + \|B\rangle)\|s_x;+\rangle$	$\frac{1}{\sqrt{2}}(\|A\rangle - \|B\rangle)\|s_x;-\rangle$
$\|\phi_{-\Delta,2}\rangle$	$\frac{1}{\sqrt{2}}(\|A\rangle + \|B\rangle)\|s_x;-\rangle$	$-\frac{1}{\sqrt{2}}(\|A\rangle + \|B\rangle)\|s_x;+\rangle$
$\|\phi_{+\Delta,1}\rangle$	$\frac{1}{\sqrt{2}}(\|A\rangle - \|B\rangle)\|s_x;-\rangle$	$\frac{1}{\sqrt{2}}(-\|A\rangle + \|B\rangle)\|s_x;+\rangle$
$\|\phi_{+\Delta,2}\rangle$	$\frac{1}{\sqrt{2}}(\|A\rangle + \|B\rangle)\|s_x;+\rangle$	$-\frac{1}{\sqrt{2}}(\|A\rangle + \|B\rangle)\|s_x;-\rangle$

Summary. We have demonstrated the structural stability of HB tin and HB lead and discussed their electronic properties, showed that tin and lead are not viable routes towards topological fullerenes, and discovered the structural, valley, sublattice, and spin properties of optimal fluorinated two-dimensional tin.

We are grateful to G. Montambaux, M. Kindermann, and L. Bellaiche and acknowledge the Arkansas Biosciences Institute (P.R. and S.B.L.); Faculty Development and Research Committee Grant No. OSPR 140269 and the FCSM Fisher General Endowment at Towson University (J.A.Y.); Spanish MICINN Grant No. FIS2012-34858 and European Commission FP7 ITN "MOLESCO" Grant No. 606728 (V.M.G.S. and J.F.); and Ramón y Cajal Fellowship No. RYC-2010-06053 (V.M.G.S.). Computations were carried out in Arkansas and at TACC (XSEDE TG-PHY090002).

[1] M. Katsnelson, *Graphene: Carbon in Two Dimensions*, 1st ed. (Cambridge University Press, Cambridge, 2012).

[2] A. H. Castro Neto, F. Guinea, N. M. R. Peres, K. S. Novoselov, and A. K. Geim, Rev. Mod. Phys. **81**, 109 (2009).

[3] S. Cahangirov, M. Topsakal, E. Aktürk, H. Sahin, and S. Ciraci, Phys. Rev. Lett. **102**, 236804 (2009).

[4] H. L. Zhuang, A. K. Singh, and R. G. Hennig, Phys. Rev. B **87**, 165415 (2013).

[5] Z. Zhu and D. Tománek, Phys. Rev. Lett. **112**, 176802 (2014).

[6] J. C. Garcia, D. B. de Lima, L. V. C. Assali, and J. F. Justo, J. Phys. Chem. C **115**, 13242 (2011).

[7] Y. Ma, Y. Dai, M. Guo, C. Niu, and B. Huang, J. Phys. Chem. C **116**, 12977 (2012).
[8] Y. Xu, B. Yan, H.-J. Zhang, J. Wang, G. Xu, P. Tang, W. Duan, and S.-C. Zhang, Phys. Rev. Lett. **111**, 136804 (2013).
[9] N. Roome and J. Carey, ACS Appl. Mater. Interfaces **6**, 7743 (2014).
[10] B. van den Broek, M. Houssa, E. Scalise, G. Pourtois, V. V. Afanas'ev, and A. Stesmans, 2D Mater. **1**, 021004 (2014).
[11] J. O. Sofo, A. S. Chaudhari, and G. D. Barber, Phys. Rev. B **75**, 153401 (2007).
[12] R. C. McDonald, H. H.-K. Hau, and K. Eriks, Inorg. Chem. **15**, 762 (1976).
[13] G. Denes, J. Pannetier, J. Lucas, and J. Y. Le Marouille, J. Solid State Chem. **30**, 335 (1979).
[14] C. L. Kane and E. J. Mele, Phys. Rev. Lett. **95**, 226801 (2005).
[15] A. Rycerz, J. Tworzydlo, and C. W. J. Beenakker, Nat. Phys. **3**, 172 (2007).
[16] D. Xiao, W. Yao, and Q. Niu, Phys. Rev. Lett. **99**, 236809 (2007).
[17] J. J. Jung, F. Zhang, Z. Quiao, and A. H. McDonald, Phys. Rev. B **84**, 075418 (2011).
[18] Y. Jiang, T. Low, K. Chang, M. I. Katsnelson, and F. Guinea, Phys. Rev. Lett. **110**, 046601 (2013).
[19] X. Xu, W. Yao, D. Xiao, and T. Heinz, Nat. Phys. **10**, 343 (2014).
[20] J. P. Perdew, K. Burke, and M. Ernzerhof, Phys. Rev. Lett. **77**, 3865 (1996).
[21] J. Soler, E. Artacho, J. Gale, A. García, J. Junquera, P. Ordejón, and D. Sánchez-Portal, J. Phys.: Condens. Matter **14**, 2745 (2002).
[22] E. Artacho, E. Anglada, O. Dieguez, J. Gale, A. García, J. Junquera, R. Martin, P. Ordejón, J. Pruneda, D. Sánchez-Portal *et al.*, J. Phys.: Condens. Matter **20**, 064208 (2008).
[23] L. Fernandez-Seivane, M. A. Oliveira, S. Sanvito, and J. Ferrer, J. Phys.: Condens. Matter **18**, 7999 (2006).
[24] P. Rivero, V. García-Suárez, Y. Yang, L. Bellaiche, K. Park, J. Ferrer, and S. Barraza-Lopez, Comp. Mat. Sci. (2014), doi: 10.1016/j.commatsci.2014.11.026.
[25] G. Kresse and J. Hafner, Phys. Rev. B **47**, 558 (1993).
[26] G. Kresse and J. Hafner, Phys. Rev. B **49**, 14251 (1994).
[27] M. Marder, *Condensed Matter Physics*, 1st ed. (Wiley-Interscience, New York, 2000).
[28] C. Sabater, D. Gosálbez-Martínez, J. Fernández-Rossier, J. G. Rodrigo, C. Untiedt, and J. J. Palacios, Phys. Rev. Lett. **110**, 176802 (2013).
[29] L. Miao, Z. F. Wang, M.-Y. Yao, F. Zhu, J. H. Dil, C. L. Gao, C. Liu, F. Liu, D. Quian, and J. F. Jia, Phys. Rev. B **89**, 155116 (2014).
[30] Phonon dispersion calculations were performed with the Vibra tool. The atomic displacements used in computing force constants were as small as 0.01 Å, we set the electronic tolerance smaller than 10^{-5} eV, and the mesh cutoff for the real-space grid was larger than 800 Ry. Large supercells were needed in order to eliminate spurious negative frequencies, and an $11 \times 11 \times 1$ ($13 \times 13 \times 1$) supercell containing 242 (338) atoms for the calculations of high-buckled tin (lead). Due to the heavier computational cost, calculations that included SOI were carried out on $9 \times 9 \times 1$ supercells, containing 162 atoms. A k-point sampling of at least $6 \times 6 \times 1$ in all phonon calculations ensures a properly converged electronic density.
[31] Phonon dispersion calculations with the QUANTUM ESPRESSO package [32] confirm these results.
[32] P. Giannozzi, S. Baroni, N. Bonini, M. Calandra, R. Car, C. Cavazzoni, D. Ceresoli, G. L. Chiarotti, M. Cococcioni, I. Dabo *et al.*, J. Phys.: Condens. Matter **21**, 395502 (2009).
[33] A. Rüegg, S. Coh, and J. E. Moore, Phys. Rev. B **88**, 155127 (2013).
[34] T. Ando, J. Phys. Soc. Jpn. **69**, 1757 (2000).
[35] D. Huertas-Hernando, F. Guinea, and A. Brataas, Phys. Rev. B **74**, 155426 (2006).
[36] C.-C. Liu, W. Feng, and Y. Yao, Phys. Rev. Lett. **107**, 076802 (2011).
[37] C.-C. Liu, H. Jiang, and Y. Yao, Phys. Rev. B **84**, 195430 (2011).
[38] A. Barfuss, L. Dudy, M. Scholz, H. Roth, P. Höpfner, C. Blumenstein, G. Landolt, J. Dil, N. Plumb, M. Radovic *et al.*, Phys. Rev. Lett. **111**, 157205 (2013).
[39] Y. Ohtsubo, P. Le Fèvre, F. Bertran, and A. Taleb-Ibrahimi, Phys. Rev. Lett. **111**, 216401 (2013).
[40] T. Miller, M. Y. Chou, and T.-C. Chiang, Phys. Rev. Lett. **102**, 236803 (2009).
[41] P. Bridman, Proc. Am. Acad. Arts Sci. **60**, 305 (1925).
[42] P. Pavone, S. Baroni, and S. de Gironcoli, Phys. Rev. B **57**, 10421 (1998).
[43] J. Chelikowsky and M. Cohen, Phys. Rev. B **14**, 556 (1976).
[44] G. Montambaux, F. Piéchon, J.-N. Fuchs, and M. O. Goerbig, Phys. Rev. B **80**, 153412 (2009).